Fontorbe, G., Frings, P., De La Rocha, C. L., Hendry, K. R., Carstensen, J., Conley, D. J. (2017): Enrichment of dissolved silica in the deep equatorial Pacific during the Eocene-Oligocene. - *Paleoceanography*, *32*, 8, pp. 848—863.

DOI: http://doi.org/10.1002/2017PA003090

AGU PUBLICATIONS

Paleoceanography

RESEARCH ARTICLE
10.1002/2017PA003090

Key Points:
- Silicon isotope composition of BSi can complement other paleocirculation proxies to assess changes in ocean circulation
- The Equatorial Pacific became more silica-rich from 37 Ma onward due to a change in the provenance of deep waters

Supporting Information:
- Supporting Information S1

Correspondence to:
G. Fontorbe,
guillaume.fontorbe@geol.lu.se

Citation:
Fontorbe, G., P. J. Frings, C. L. De La Rocha, K. R. Hendry, J. Carstensen, and D. J. Conley (2017), Enrichment of dissolved silica in the deep equatorial Pacific during the Eocene-Oligocene, *Paleoceanography*, *32*, 848–863, doi:10.1002/2017PA003090.

Received 19 JAN 2017
Accepted 28 JUL 2017
Accepted article online 3 AUG 2017
Published online 18 AUG 2017

Enrichment of dissolved silica in the deep equatorial Pacific during the Eocene-Oligocene

Guillaume Fontorbe[1], Patrick J. Frings[1,2,3], Christina L. De La Rocha[1], Katharine R. Hendry[4], Jacob Carstensen[5], and Daniel J. Conley[1]

[1]Department of Geology, Lund University, Lund, Sweden, [2]Now at Department of Geoscience Swedish Museum of Natural History, Stockholm, Sweden, [3]Earth Surface Geochemistry, Helmholtz Centre Potsdam GFZ German Research Centre for Geosciences, Potsdam, Germany, [4]School of Earth Sciences, University of Bristol, Bristol, UK, [5]Department of Bioscience, Aarhus University, Roskilde, Denmark

Abstract Silicon isotope ratios (expressed as δ^{30}Si) in marine microfossils can provide insights into silica cycling over geologic time. Here we used δ^{30}Si of sponge spicules and radiolarian tests from the Paleogene Equatorial Transect (Ocean Drilling Program Leg 199) spanning the Eocene and Oligocene (~50–23 Ma) to reconstruct dissolved silica (DSi) concentrations in deep waters and to examine upper ocean δ^{30}Si. The δ^{30}Si values range from −3.16 to +0.18‰ and from −0.07 to +1.42‰ for the sponge and radiolarian records, respectively. Both records show a transition toward lower δ^{30}Si values around 37 Ma. The shift in radiolarian δ^{30}Si is interpreted as a consequence of changes in the δ^{30}Si of source DSi to the region. The decrease in sponge δ^{30}Si is interpreted as a transition from low DSi concentrations to higher DSi concentrations, most likely related to the shift toward a solely Southern Ocean source of deep water in the Pacific during the Paleogene that has been suggested by results from paleoceanographic tracers such as neodymium and carbon isotopes. Sponge δ^{30}Si provides relatively direct information about the nutrient content of deep water and is a useful complement to other tracers of deep water circulation in the oceans of the past.

1. Introduction

The interplay of nutrient uptake, biomineralization, remineralization, and dissolution with ocean circulation defines the distribution of nutrients in the ocean. For the macronutrient Si, biogenic silica (BSi) formation in surface waters by diatoms—and radiolarians, to a lesser extent—and their progressive dissolution during sinking creates a global surface/deep gradient in dissolved Si (DSi) concentrations. This is superimposed on an interbasin DSi gradient, where newly formed deep water (e.g., North Atlantic Deep Water) has little Si but older water masses (e.g., North Pacific Deep Water) have had sufficient time to accumulate Si from dissolution of sinking BSi [e.g., *Garcia et al*., 2014; *de Souza et al*., 2014].

An entirely different situation prevailed in the early Paleogene (Paleocene and Early Eocene, ~65–50 Ma). Exchange between the Atlantic and Pacific Oceans was restricted [*Thomas et al*., 2003], and formation of deep water potentially took place at high latitudes in both hemispheres in each basin. Global climate and carbon cycling transitioned from greenhouse toward icehouse conditions from the mid-Paleogene (50 Ma) onward as a series of several stepwise changes superimposed on a longer-term cooling trend and interspersed with transient perturbations [*Zachos et al*., 2001]. This general cooling trend and some transient events have been attributed to tectonic activity impacting the paleogeography and global ocean circulation [*Raymo and Ruddiman*, 1992].

Perhaps the most important of these steps occurred at the Eocene/Oligocene boundary (33.9 Ma) with evidence for the establishment of permanent continental ice sheets on Antarctica [e.g., *Zachos and Kump*, 2005; *Lear et al*., 2008] and changes in continental weathering regimes [e.g., *Raymo and Ruddiman*, 1992; *Zachos et al*., 1999]. Major biotic changes also occur throughout the Cenozoic, notably including the evolutionary expansion of the diatoms [*Rabosky and Sorhannus*, 2009], as well as numerous plate tectonic events that resulted in volcanism, mountain building, and the opening or closing of ocean gateways [e.g., *Garzione*, 2008]. For example, the subsidence of Antarctic land bridges apparently reinforced the strength of the Antarctic Circumpolar Current and the formation of deep waters in the Pacific sector of the Southern Ocean, ultimately leading to the cessation of deepwater formation in the North Pacific during the Middle Eocene (~42 Ma) [*Thomas et al*., 2008]. All these events could impact the supply of DSi to different regions

of the ocean via changing deepwater circulation, vertical stratification, or even the overall production and export of biogenic silica on local to global scales. Essentially, the oceanic distribution of DSi and ocean circulation are tightly linked [*de Souza et al*., 2014]. Study of the marine Si cycling during periods of major ocean circulation reorganization such as the Eocene/Oligocene boundary can shed light onto the evolution of past nutrient dynamics and ocean evolution.

The silicon isotopic composition of biogenic silica (BSi) extracted from sediments can be used to investigate these issues because biological uptake of Si fractionates the stable isotopes ^{28}Si, ^{29}Si, and ^{30}Si. The uptake of dissolved silicon (DSi) from the surrounding water and precipitation as BSi discriminates against the heavier isotopes of silicon, resulting in the BSi being isotopically lighter than the DSi from which it derives [*De La Rocha et al*., 1997]. Differences in the habitat and Si metabolism of the three main groups of marine silicifying organisms—diatoms, radiolarians, and sponges—gives rise to a multifaceted silicon isotope toolkit that can be used to investigate aspects of the oceanic Si cycle. Si isotope ratios (expressed as δ^{30}Si) in diatom frustules are used to estimate the degree of Si utilization in surface waters [e.g., *Cardinal et al*., 2005; *Coffineau et al*., 2014; *De La Rocha et al*., 1998; *Egan et al*., 2012; *Varela et al*., 2004]. Conversely, radiolarians, which are heterotrophs, do not generally utilize a large fraction of the available Si. Radiolarian δ^{30}Si should therefore more passively track the silicon isotopic composition of the upper couple of hundred meters of the water column [*Abelmann et al*., 2015; *Hendry et al*., 2014]. Finally, sponges are sessile and benthic animals; siliceous sponge spicule δ^{30}Si can be used to infer DSi concentrations at the seafloor by exploiting the observed increase in Si isotope fractionation with increasing DSi concentrations [*Hendry and Robinson*, 2012; *Wille et al*., 2010]. Overall, sedimentary siliceous remains represent a rich and almost entirely unexploited archive of paleoceanographic data.

Of particular promise is the recognition of the relationship between ambient DSi concentrations and the magnitude of sponge Si isotope fractionation (approximated as the difference between sponge δ^{30}Si and DSi δ^{30}Si, $\Delta\delta^{30}Si_{spo\text{-}DSi}$). This has opened the door to quantitative reconstructions of past DSi concentrations [*Hendry and Robinson*, 2012; *Wille et al*., 2010]. Though not fully mechanistically understood, the relationship is interpreted as resulting from the expression of only Si isotope fractionation during uptake at high influx/efflux ratios (low concentrations), while fractionation associated with uptake, precipitation, and efflux can all be (additively) expressed at low influx/efflux ratios (high concentrations) [*Hendry and Robinson*, 2012; *Wille et al*., 2010]. The first application of this proxy to Cenozoic timescales [*Fontorbe et al*., 2016] suggested that DSi concentrations in the deeper waters of the North Atlantic were remarkably similar to modern values during the Paleocene and Eocene, i.e., from 60 Ma onward. This is a surprising result, since conventional wisdom dictated that diatom radiation in the early Cenozoic caused a period of transition from a DSi-repleted to DSi-depleted ocean (i.e., from ~600–1100 μM to the modern 0–200 μM) [*Maliva et al*., 1989; *Siever*, 1991; *Lazarus et al*., 2009]. The results of *Fontorbe et al*. [2016] require that the transition to a low Si North Atlantic had begun prior the early Cenozoic (i.e., prior to 60 Ma).

One key aspect missing from the picture is a constraint on the timing, duration, and global synchrony of any transition to the modern low DSi ocean. This leaves the question open for other ocean basins. Were DSi concentrations already at modern levels in all basins during the Paleogene and, if not, how different were they? Using a similar approach to *Fontorbe et al*. [2016], this study aims to reconstruct bottom water DSi concentrations and δ^{30}Si of surface to middepth waters in the Equatorial Pacific during the Eocene and Oligocene.

Such an exercise is valuable for two main reasons. First, it helps shed light on the evolution of the marine Si cycle. As mentioned above, this remains poorly constrained even for the relatively recent period from the late Mesozoic onward (i.e., 150 Ma to present). Second, as we argue below, the ability to derive paleo-DSi concentrations from sponge spicule δ^{30}Si analysis serves as a useful proxy for water mass age and therefore paleocirculation. Silicon isotopes are thus well placed to address outstanding issues regarding the interactions of tectonics, climate, biogeochemistry, and ocean circulation.

2. Materials and Method

2.1. Site Description

A total of 75 samples from Ocean Drilling Program (ODP) sites 1217 to 1221 from the Paleogene equatorial transect (ODP Leg 199; ~7–16°N, 135–143°W, Figure 1a, Table 1) were selected for silicon isotope analysis.

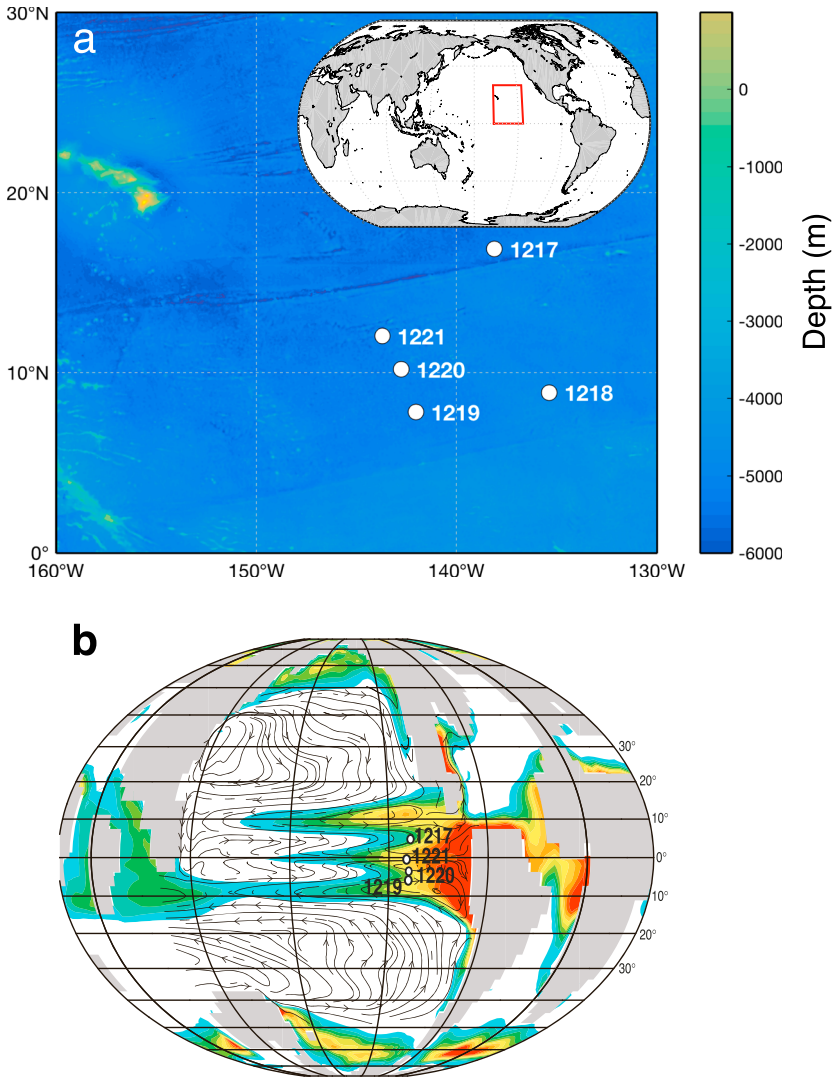

Figure 1. (a) Modern location of the drill sites from ODP Leg 199. Map generated using ETOPO1 dataset [*Amante and Eakins*, 2009]. (b) Mollweide projection of global land-sea distribution during the early Paleogene and modeled annual average upwelling into the thermocline. Red indicates areas of vigorous upwelling, blue/green indicates regions of weak upwelling, and white indicates areas of mean downwelling. Streamlines are shown for a 100 m depth. Sites locations correspond to the position during the early Paleogene. Physical model from *Huber* [2002].

The stratigraphic sequence sampled is composed mostly of early Eocene to late Oligocene (~49 to 23 Ma) radiolarian and nannofossil oozes. The age models are derived from magnetostratigraphy combined with nannofossil, foraminifer, and radiolarian biostratigraphic markers (as detailed in *Lyle et al.* [2002]). The modern-day eastern equatorial Pacific is highly influenced by upwelling that brings deep waters to the surface, stimulating productivity that results in a band of highly biogenic sedimentation accumulating within a couple degrees along the equator. Coupled atmospheric-ocean circulation models have reconstructed Equatorial Pacific upwelling annual intensity during the early Paleogene [*Huber*, 2002] and suggested that drilled sites during ODP Leg 199 were inside the upwelling influenced area during the Paleogene. Figure 1b shows the zone under upwelling influence during the early Paleogene and the approximate paleolocation of the cores.

Modern surface DSi concentrations at the location of Paleogene sediment deposition (~5°S–5°N, 130–150°W, Figure 1) are low, ranging from ~0 to ~10 μM [*Garcia et al.*, 2014]. Concentrations gradually increase with depth up to ~50 μM in the top 500 m and to >150 μM below 1000 m [*Garcia et al.*, 2014]. Measurements

Table 1. Modern Locations, Water Depths, Sampled Intervals, Approximate Age Interval [*Lyle et al*., 2002], and Number of Samples for Each Individual Hole Sampled[a]

Hole	Modern Location	Water Depth (mbsl)	Sampled Interval (mbsf)	Approx. Age Range (Ma)	Number of Samples
1217 A	16°52.0133′N 138°05.9981′W	5342.1	30–86	33–45	11
1217 B	16°52.0175′N 138°06.0007′W	5342.1	30–84	34–44	12
1218 A	08°53.3667′N 135°22.0002′W	4826.3	77–260	23–41	15
1219 A	7°48.0097′N 142°00.9390′W	5063.3	56–221	24–56	16
1220 A	10°10.6008′N 142°45.4917′W	5217.9	40–114	28–42	8
1221 A	12°01.9987′N 143°41.6514′W	5175.3	10–113	32–48	13

[a]mbsl, meters below sea level; mbsf, meters below sea floor.

of the silicon isotopic composition of DSi in the upper 200 m of the equatorial Pacific range from +1.2 to +4.4‰, depending on the degree of biological utilization [*Beucher et al*., 2008, 2011; *de Souza et al*., 2012; *Grasse et al*., 2013]. The heaviest Si isotopic signatures are found in Si-depleted waters (~0.2 μM) [*Grasse et al*., 2013] which result from high biological production preferentially removing the lighter Si isotopes. Modern $\delta^{30}Si_{DSi}$ values in the deep equatorial Pacific are fairly invariant and range from ~+1.2 to +1.5‰ [*Beucher et al*., 2008, 2011].

2.2. Sample Preparation

Biogenic silica was physically separated from other sediment components using standard techniques [*Morley et al*., 2004]. Briefly, sediments were cleaned with hydrochloric acid and hydrogen peroxide to remove carbonates and organic matter, respectively. BSi was then separated from lithogenic silicates and clays by repeated density separation using a sodium polytungstate solution with a density between 2.1 and 2.3 g/mL. The light fraction recovered (i.e., the fraction containing biogenic silica) was wet sieved at 53 μm to remove the majority of fragmented material and isolate sponge spicules and intact radiolarian tests.

From this cleaned fraction, monoaxonic sponge spicules and radiolarian tests were handpicked under a light microscope to minimize contamination from unwanted particles. For example, the selection of only monoaxonic spicules (i.e., a class of spicule with silica precipitated along a single axis, common to most siliceous sponges) minimized any potential contribution of spicule type to silicon isotope variations [*Hendry et al*., 2015]. Meanwhile, the radiolarian test samples were picked to represent a bulk radiolarian community. Benefits and drawbacks induced by the selection of a bulk radiolarian community are discussed below. The separated and handpicked BSi was then dissolved in 0.4 M NaOH in microcentrifuge tubes for a minimum of 3 days at 100°C, acidified with HNO_3 to pH around 2, and purified chromatographically through a cation exchange resin following *Georg et al*. [2006a] for silicon isotope ratio analysis. Full procedural blanks were processed throughout and contributed less than 1% of the beam intensity of a typical sample during analysis.

2.3. Silicon Isotope Analysis

The silicon isotopic composition of the purified Si solutions was determined using a multicollector inductively coupled plasma mass spectrometer (Neptune, Thermo Scientific) at the Pole Spectrometrie Ocean (Ifremer, Brest). The Si solutions as well as the standards, diluted to 2 ppm using 1% HNO_3, were introduced through an APEX-HF (ESI) desolvator, PFA nebulizer (50 μL/min), and an alumina injector. The signal intensity was in the vicinity of 25 V on mass 28 at medium resolution. An internal Mg standard with matching concentration (2 ppm) was added to each standard and sample to correct from instrumental mass bias. Beam intensities on masses 28, 29, and 30 for silicon and on masses 25 and 26 for magnesium were monitored for a block of 25 cycles of 15 s, followed by a 1% HNO_3 rinse for 3 min. Measured magnesium isotope ratios were used to monitor and correct for instrumental mass bias using an exponential law, after *Cardinal et al*. [2003]. The beam intensity on mass 28 during the rinse and procedural blanks was $<$1% of the standards and samples beam intensity.The silicon isotope ratios are given relative to a

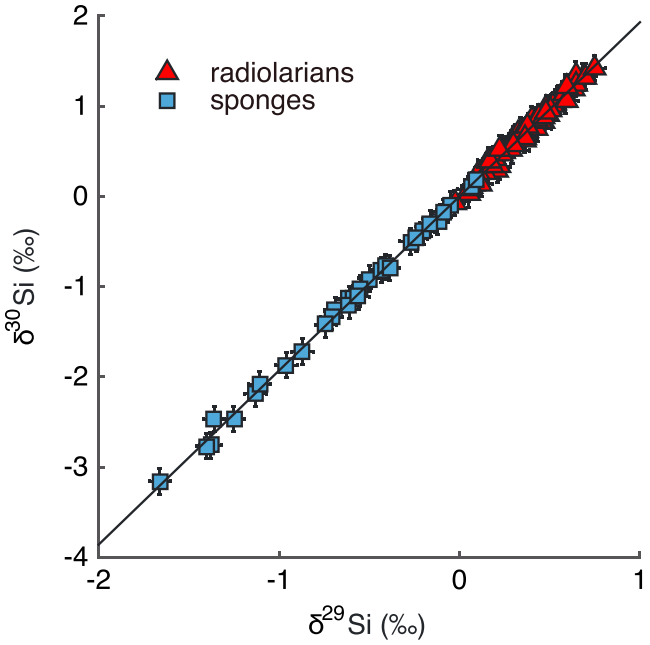

Figure 2. Three-isotope plot (δ^{30}Si versus δ^{29}Si) of radiolarian tests (red triangles) and sponge spicules (blue squares). The data fall on the expected mass-dependent equilibrium fractionation (black line: $\delta^{30}Si = 1.93 \times \delta^{29}Si$, $r^2 = 0.998$, $n = 105$). Vertical and horizontal bars represent long-term precision (expressed as 2σ).

standard (NBS28, National Institute of Standards and Technology) as δ^xSi values corresponding to an average of two series of bracketed measurements (i.e., 2 blocks of standard sample standard):

$$\delta^x Si = \left(\frac{R_{sam}}{R_{std}} - 1\right) \times 1000 \quad (1)$$

where R_{sam} and R_{std} is the corrected ratio of ^{x}Si/^{28}Si of the sample and the standard, respectively. Values fall on the expected mass-dependent fractionation line $\delta^{30}Si = 1.93 \times \delta^{29}Si$ ($r^2 = 0.998$, $n = 105$, Figure 2), demonstrating the successful removal of polyatomic interferences during measurement. δ^{30}Si analyses on secondary standards Big Batch and Diatomite prepared using identical methods and measured during the same analytical sessions yielded values in agreement with accepted values [*Reynolds et al.*, 2007] (supporting information Table S1). Long-term precision (expressed as 2σ), based on measurements of multiple NBS28 standards and secondary standards, was of ±0.14‰ for δ^{30}Si and ±0.06‰ for δ^{29}Si.

2.4. Statistical Analyses

Stratigraphic time series of δ^{30}Si for radiolarian tests and sponge spicule samples were analyzed for change points over time using a combination of abrupt step changes and piecewise linear regressions [*Carstensen and Weydmann*, 2012]. The abrupt step change model has a discontinuity where the mean of the stratigraphic sequence changes from one time point to another, whereas the piecewise linear regression is continuous with line segments connected at different time points that are also estimated. An autoregressive term (AR(1) process) for the error process is included in the change point analyses to describe potential correlation in the stratigraphic sequence, accounting for the nonequidistant distribution over time. Nonsignificant slopes in the piecewise linear model are set to zero. The significance of the change point models is assessed using likelihood ratio statistics, and the abrupt and piecewise linear models are compared using Bayes information criterion (BIC). The change point detection analyses are carried out using PROC MODEL in SAS v.9.3.

3. Results

The 75 radiolarian samples covering 23.1 to 47.9 Ma have δ^{30}Si values ranging from −0.07 to +1.42‰. The 30 sponge spicule samples, covering this same time interval, have consistently lower values, ranging from −3.16 to +0.18‰. The time resolution discrepancy between the radiolarian and the sponge records is due to insufficient sponge spicules in some samples. All data are presented in supporting information Table S1. The range of δ^{30}Si values for the radiolarians agrees well with previous work on the Paleocene-Eocene Atlantic Ocean (δ^{30}Si from +0.32 to +1.67‰, $n = 65$) [*Fontorbe et al.*, 2016] and overlaps with the upper range of values (−0.90 to 1.17‰) in the Atlantic sector of the Southern Ocean from the past 30 ka [*Abelmann et al.*, 2015] and from the Heinrich Stadial 1 (~17 ka) in the North Atlantic (+0.73 to +2.00‰,) [*Hendry et al.*, 2014].

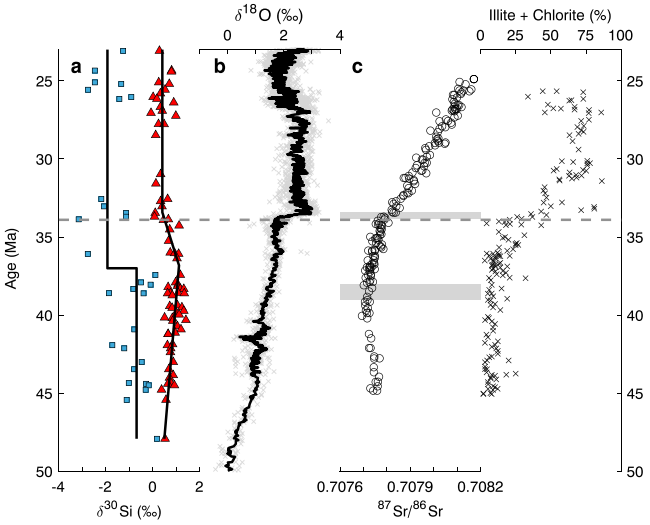

Figure 3. (a) Radiolarian (red triangles) and sponge (blue squares) δ^{30}Si in the equatorial Pacific during the Eocene and Oligocene. Thick black lines show local mean values and trends (see section 2.4). (b) Global composite benthic foraminifera δ^{18}O from *Zachos et al.* [2001]. (c) Planktonic foraminifera ^{87}Sr/^{86}Sr ratios from deep sea Southern Ocean sediments. Shaded areas show periods of significant slope change. From *Zachos et al.* [1999]. (d) Proportion of illite and chlorite in Southern Ocean marine sediments [*Ehrmann and Mackensen*, 1992]. Horizontal dashed line shows the Eocene/Oligocene boundary.

A piecewise linear regression with two breakpoints (see section 2.4) better describes the variations in the radiolarian δ^{30}Si records (BIC = 22.2 and 35.9, respectively) than the abrupt step change model. The autoregressive term is not significant for any of these two models. Three distinct periods emerge from the analysis (Figure 3a). First, the record gradually increases between ~48 and 37 Ma (+0.06‰ per mega annum; P = 0.0420). The second period is characterized by a faster decrease from ~37 to 33 Ma (−0.21‰ per mega annum; P = 0.0305), before the record reaches a constant level around +0.41‰.

The sponge record is best described with an abrupt step change model (BIC = 65.7 versus 74.0 for a linear regression, i.e., no significant breakpoints in the piecewise linear regression), separating two distinct periods. The autoregressive term is not significant for either of the two model types. The first period falls between 48 and 37 Ma and has δ^{30}Si values of 0 to −1‰, similar to those of modern sponges living at low DSi concentrations (i.e., [DSi] < 25 μM) [*Hendry and Robinson*, 2012; *Wille et al.*, 2010]. Following this, there is a transition to lower δ^{30}Si values (between −1 and −2‰) for the rest of the sponge record (Figure 3a). These values are higher than sponge δ^{30}Si values published for the Southern Ocean over the Eocene-Oligocene transition [*De La Rocha*, 2003; *Egan et al.*, 2013] and consistently lower than reported values in the Atlantic Ocean during the Paleocene and Eocene [*Fontorbe et al.*, 2016].

4. Discussion

4.1. A Critical Look at the Use of BSi δ^{30}Si

The use of radiolarian δ^{30}Si, and to a lesser extent sponge δ^{30}Si, as proxies for aspects of the paleo-Si cycle is at an early stage. Consequently, one should consider the potential influence of diagenesis and dissolution on the fidelity of the sedimentary δ^{30}Si record. One should also be aware of the extent to which our poor understanding of Si isotope fractionation during the precipitation of radiolarian tests limits our interpretive ability.

4.1.1. Diagenetic Overprinting

A first concern is the impact of diagenetic processes on opal δ^{30}Si. The transformation of opal-A produced by siliceous organisms to opal-CT occurs via a series of dissolution and reprecipitation reactions that are associated with fractionation of Si isotopes [*Tatzel et al.*, 2015]. The extent to which this fractionation is manifest depends on the completeness of the transformation. *Marin-Carbonne et al.* [2014] demonstrated that this process complicates chert δ^{30}Si interpretation. However, neither light microscopy nor scanning electron microscopy revealed any sign of extensive dissolution or reprecipitation. Crucially, diagenetic processes would tend to homogenize the δ^{30}Si of the BSi fractions, yet we see interfraction δ^{30}Si differences of up to ~3‰. Further, analysis by X-Ray diffraction of sponge spicules from the Eocene/Oligocene boundary extracted from deep-sea sediments in the Atlantic sector of the Southern Ocean [*De La Rocha*, 2003] suggested that the spicules were still dominantly composed of opal-A, i.e., they had not yet undergone diagenetic recrystallization. In any case, the few occurrences of porcellanite—a form of opal CT—present in the

sediment sequence [*Lyle et al*., 2002] have intentionally been left unsampled. Consequently, it seems unlikely diagenetic artifacts substantially affect our δ^{30}Si records.

4.1.2. BSi Dissolution

A second process to consider is the dissolution of BSi and any potential isotopic impact on the residual BSi. *Demarest et al*. [2009], in a study on diatom BSi dissolution under closed conditions, reported the preferential release of lighter Si isotopes during dissolution with a Si isotope enrichment $^{30}\varepsilon_{diss}$ of −0.55‰. This is a non-negligible fraction of total BSi δ^{30}Si variability in Paleogene sediments [*Egan et al*., 2013; *Fontorbe et al*., 2016; this study]. In a more recent study, *Wetzel et al*. [2014] did not observe significant Si isotope fractionation during dissolution of diatom opal and argued for the robustness of $\delta^{30}Si_{BSi}$ in the deep-sea sedimentary environment against dissolution. Since dissolution is a surface process, mass balance dictates that fractionation cannot be maintained definitely. Conceptually, a surface layer may become compositionally distinct but must be removed entirely (negating the potential for fractionation) before the next layer can dissolve. In line with this, *Sun et al*. [2014] noted fractionation of Si isotopes during the early stage of dissolution of diatom BSi in brackish waters. However, this fractionation was expressed only in DSi whereas the Si isotope signature of BSi remained unchanged. In general, all previous work highlights that a considerable proportion of BSi has to dissolve in order to produce a measurable effect on the δ^{30}Si of the residual opal. Furthermore, several water column, sediment trap, or core top studies attest to the absence of observable isotopic fractionation in natural settings [e.g., *Egan et al*., 2012; *Fripiat et al*., 2011; *Panizzo et al*., 2016]. For example, *Panizzo et al*. [2016] demonstrated the absence of fractionation of diatom Si isotopes during sinking and early burial in Lake Baikal. As noted above, our microscopic observations as well as focused studies on the radiolarian fauna [*Funakawa et al*., 2006; *Kamikuri et al*., 2005] do not reveal signs of dissolution, corroborating the minor impact of BSi dissolution on our δ^{30}Si records.

4.1.3. Interpretation of Radiolarian δ^{30}Si

Radiolarians are not easily maintained in cultures through a reproductive cycle [*Krabberød et al*., 2011], so the study of Si isotope fractionation during formation of new radiolarian tests under controlled conditions is not yet possible. Radiolarian tests are thought to precipitate after internal concentration of Si that has been taken up across the outer cell membrane and transported to specialized membranes that control Si deposition [*Wallace et al*., 2012]. As with sponges, the isotope fractionations associated with uptake, internal transport, deposition, and efflux could create a relationship between ambient DSi concentrations and the net Si isotope fractionation if they are variably expressed. However, the extent of Si efflux—and thus variable expression of Si isotope fractionation—is not yet resolved. In general, it is assumed that fractionation by radiolarians will be unaffected by external DSi concentration. In the absence of evidence for a relationship between Si isotope fractionation during the formation of radiolarian test and ambient DSi concentration, we hypothesize that radiolarian δ^{30}Si tracks the isotopic composition—with a fractionation induced offset—of the source DSi. No study of the potential for species-specific Si isotope fractionation, as recently demonstrated for diatoms [*Sutton et al*., 2013], exists for radiolarians. *Abelmann et al*. [2015] observed a difference in radiolarian δ^{30}Si between the 125–250 and >250 μm size fractions of up to 1.5‰. However, they could not attribute this to either species-specific Si isotope fractionation (i.e., "physiological effects") or to different depth habitats (and hence different source DSi δ^{30}Si). Our conscious choice to select all radiolarian species during sample preparation should tend to average out the influence, if any, of species-specific Si isotope fractionation and depth habitat. We acknowledge the potential for bias to be introduced by shifts in radiolarian species and associated Si isotope fractionation but consider that our data still hold relevant information for reconstructing silicon cycling over geological timescales.

4.2. Silicon Isotopic Composition of Equatorial Pacific Surface Waters

Radiolarians dwell in the upper few hundred meters of the water column. Estimates of silicon isotopic fractionation by radiolarians cluster around values similar to diatoms. *Hendry et al*. [2014] inferred an offset of −1.1 to −2.1‰ between radiolarian silica and DSi in the Sargasso Sea, based on comparison with diatom δ^{30}Si record during the most recent Heinrich Stadial (15–17 ka). Based on core top analyses, *Abelmann et al*. [2015] derived similar values of −0.8 to −1.5‰ for their reconstructions. We use *Abelmann et al*.'s [2015] more constrained range of offset between radiolarian silica and seawater ($-1.5 < \Delta\delta^{30}Si < -0.8$‰) to reconstruct δ^{30}Si of DSi during the Paleogene in the equatorial Pacific. The reconstructed δ^{30}Si of DSi thus corresponds to the δ^{30}Si of radiolarian tests to which we add the enrichment parameter $\varepsilon_{rad\text{-}DSi}$ (i.e.,

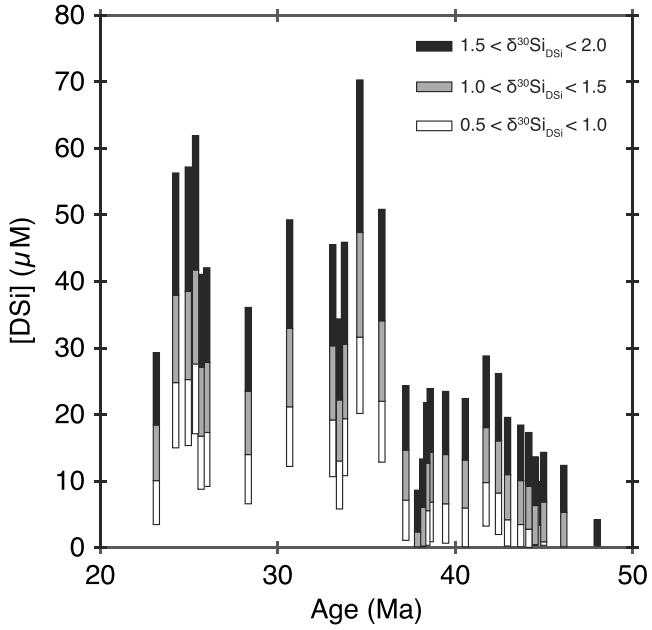

Figure 4. Reconstructed bottom waters DSi concentrations calculated following equation (3), according to three prescribed intervals of $\delta^{30}Si_{DSi}$. (+0.5 to +1.0‰, white bars; +1.0‰ to +1.5‰, gray bars; +1.5 to +2.0‰, black bars).

$\delta^{30}Si_{DSi} = \delta^{30}Si_{rad} + \varepsilon_{rad\text{-}DSi}$), in per mil. Paleogene δ^{30}Si of DSi thus varies between +0.97 to +2.70‰, in good agreement with published data for the upper few hundred meters of the modern Pacific Ocean [e.g., *Beucher et al*., 2008, 2011; *De La Rocha et al*., 2000; *de Souza et al*., 2014; *Grasse et al*., 2013; *Reynolds et al*., 2006]. From this, we suggest that the Si isotopic composition of DSi in the upper equatorial Pacific during the Paleogene was within a similar range to that observed today.

4.3. Reconstruction of Bottom Water DSi Concentrations

Si isotopes in sponge spicules can be used to infer DSi concentration [*Wille et al*., 2010; *Hendry and Robinson*, 2012]. Two comparable models exist in the literature that relate the magnitude of the fractionation between the BSi formed by the precipitation of siliceous sponge spicules and the DSi concentration of the ambient seawater [*Wille et al*., 2010; *Hendry and Robinson*, 2012]. Both models describe an asymptotic inverse relationship between the extent of Si isotope fractionation and DSi concentration in the surrounding waters. *Wille et al*. [2010] estimated a maximum fractionation of −6.02‰ at high DSi concentrations, while *Hendry and Robinson* [2012] give a slightly greater magnitude asymptote of −6.28‰. We use the latter model due to the larger data set (which includes the data of *Wille et al*. [2010]) with better geographical coverage. The calibrated relationship between Si isotope fractionation during the formation of sponge spicules and ambient DSi concentration is given as follows:

$$\Delta\delta^{30}Si_{spo-DSi} = -6.54 + \frac{270}{53 + [DSi]} \quad (2)$$

where $\Delta\delta^{30}Si_{spo\text{-}DSi}$ is the fractionation in per mil between core top sponge spicules and seawater (i.e., $\Delta\delta^{30}Si_{spo\text{-}DSi} = \delta^{30}Si_{spo} - \delta^{30}Si_{DSi}$) and [DSi] is the ambient concentration in μM and the coefficients are empirical fits to the data. In the modern ocean, the δ^{30}Si of DSi in waters deeper than 1000 m ranges from +0.5 to +2‰ [e.g., *de Souza et al*., 2014]. Using this range, we can calculate the possible DSi concentrations associated with any given spicule δ^{30}Si. Rearranging equation (2) for DSi concentrations yields

$$[DSi] = \frac{270}{\delta^{30}Si_{spo} - \delta^{30}Si_{DSi} + 6.54} - 53 \quad (3)$$

Assuming realistic values for Pacific δ^{30}Si between +0.5 and +2‰, physically plausible DSi concentrations reconstructed from the sponge spicule record range from ~0 to ~20–30 μM prior to 37 Ma and from between ~10–20 to 50–70 μM after 37 Ma (Figure 4).

The reconstruction is sensitive at low concentrations of DSi, yielding a relatively precise estimate of DSi δ^{30}Si. But the asymptotic form of the relationship between DSi concentration and sponge Si isotope fractionation limits its utility at higher DSi, such that reconstructions of high concentrations reflect more a minimum

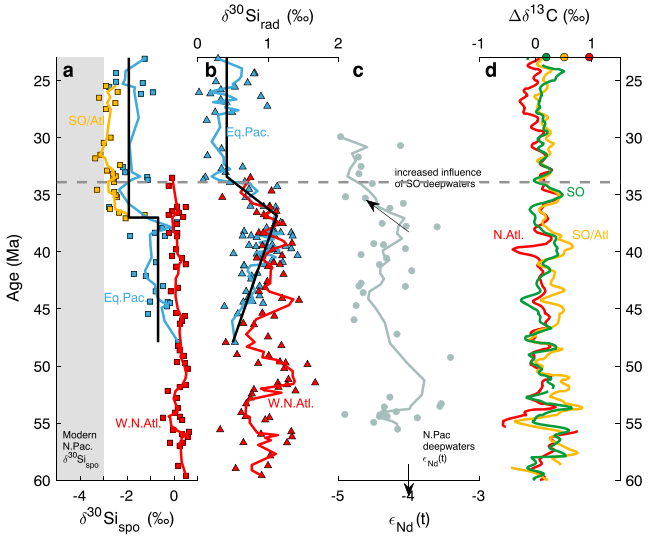

Figure 5. All available Paleogene Si isotope data and literature data for Nd at Leg 199 sites and composite C isotopic composition. (a) Sponge δ^{30}Si isotope values from the equatorial Pacific (blue line; this study), the Western North Atlantic (red line) [*Fontorbe et al*., 2016] and the Atlantic sector of the Southern Ocean (yellow line) [*Egan et al*., 2013]. The gray shaded area highlights modern range of sponge δ^{30}Si in the North Pacific [*Hendry and Robinson*, 2012]. (b) Radiolarian δ^{30}Si from the equatorial Pacific (blue line; this study), and the Western North Atlantic (red line) [*Fontorbe et al*., 2016]. (c) Nd isotope data ($\varepsilon_{Nd}(t)$) from ODP leg 199 from *Thomas et al*. [2008]. (d) Basin-specific gradient of δ^{13}C relative to the North Pacific (red line, North Atlantic; yellow line, Atlantic sector of the Southern Ocean; and green line, Southern Ocean). Colored circles indicate the modern values of the δ^{13}C gradient between the North Atlantic (red), the Atlantic sector of the Southern Ocean (yellow), and the Southern Ocean (green) and the North Pacific. Carbon stable isotope data compiled in *Cramer et al*. [2009]. Horizontal dashed line shows the E/O boundary.

possible concentration than a well-constrained estimate. However, our new spicule δ^{30}Si record still provides valuable information, especially as there is yet no other proxy for past DSi concentrations. Even with these caveats, the data indicate that Pacific deep-water DSi concentrations were lower prior to 37 Ma than after. Interpretation and implications of increasing concentrations during the latter half of the Paleogene in the equatorial Pacific are discussed further in section 4.5.

4.4. Results From Previous Studies

To our knowledge, only two studies have attempted to reconstruct aspects of the silicon cycle during the Paleogene from δ^{30}Si variations in marine microfossils. The first investigated the isotopic composition of sponge spicules and diatom frustules over the Eocene-Oligocene transition in the Southern Ocean and its Atlantic sector (ODP sites 177-1090B and 113-689B) [*Egan et al*., 2013]. Sponge spicule δ^{30}Si decreased by about 1.5‰ over a 5.5 Ma interval (37 to 31.5 Ma). The timing of this decrease corresponds well with subsidence of Southern Ocean land bridges and the opening of the Tasman Gateway and Drake Passage that led to a reorganization of Southern Ocean deepwater circulation. *Egan et al*. [2013] concluded that this change in ocean circulation resulted in a doubling of DSi concentrations in the studied area. The second study [*Fontorbe et al*., 2016] investigated Si isotope variations in sponges and radiolarians over the Paleocene and Eocene periods in the Western North Atlantic Ocean (ODP Leg 171B) and argued for a low DSi North Atlantic since the early Paleogene (from 60 Ma). Reconstruction of DSi above 50–60 μM was not supported by the data, even when assuming extreme values for the δ^{30}Si of the source DSi. A compilation of our data and previous studies can be found in Figure 5.

4.5. Potential Impact of Continental Weathering

The marine Si isotope budget is essentially a balance between low δ^{30}Si hydrothermal fluids and higher δ^{30}Si river waters. If hydrothermal activity remained relatively constant over the Cenozoic [*Rowley*, 2002], then ocean δ^{30}Si can have varied by changing the flux of continental Si and/or its mean δ^{30}Si. The Middle Cenozoic is a period of dramatic global cooling, orogenic activity, and biological innovation, cumulatively altering the boundary conditions of the terrestrial Si cycle. In a review of continental Si cycling over glacial-interglacial cycles, *Frings et al*. [2016] argue that variability in the continental Si cycle on millennial or greater timescales is sufficient to substantially alter the magnitude and δ^{30}Si of Si delivered to the ocean. Given the relatively short ocean residence time of Si (~10–12 ka) [*Frings et al*., 2016], Cenozoic biosiliceous δ^{30}Si records are sensitive to variations in the δ^{30}Si of DSi delivered to the ocean. This poses the question of whether changes to the rate or style of continental silicate weathering can explain some or all of the Leg 199 radiolarian and sponge δ^{30}Si data.

To answer this question, a first observation is that the drops in sponge and radiolarian δ^{30}Si are neither of equal magnitude nor coeval (~2‰ at 37 Ma and ~0.5‰ at 34 Ma, respectively). A second observation is that the sponge δ^{30}Si record is best described by two periods of constant δ^{30}Si offset by $>$1‰. Both of these observations argue against a whole ocean δ^{30}Si shift, which would (i) affect both equally and (ii) likely be $<$1‰. Nevertheless, both the long-term Cenozoic cooling and the onset of Antarctic glaciation around the E/O have been related to changing silicate weathering rates and CO_2 removal [e.g., *Raymo and Ruddiman*, 1992; *Zachos and Kump*, 2005]. In the following we explore in more detail how these inferred weathering changes may impact the global Si cycle.

For both the gradual Cenozoic cooling and the more abrupt onset of Antarctic glaciation, the central concept is the same: Himalayan orogeny (or some other change to global "weatherability") increases weathering rates, withdrawing CO_2 from the atmosphere and causing cooling—and glaciation, once a temperature threshold is crossed [*DeConto and Pollard*, 2003]. Support for these hypotheses comes primarily from marine $^{87}Sr/^{86}Sr$ isotope ratios as recorded in planktonic foraminifera that crudely reflect the proportional supply of Sr from continental crust and upper mantle [*Palmer and Elderfield*, 1985]. The $^{87}Sr/^{86}Sr$ record shows two major inflections around the E/O, interpreted as reflecting changes in global weathering (Figure 3c) [*Zachos et al*., 1999]. A relatively subtle inflection occurs at ~39 Ma, about 2 Ma prior to the sponge and radiolarian δ^{30}Si shift (~37 Ma, Figure 3a). A second, more marked change occurs between 33 and 34 Ma. This second change occurs broadly simultaneously with benthic foraminifera δ^{18}O and Mg/Ca shifts [e.g., *Raymo and Ruddiman*, 1992; *Zachos et al*., 2001; *Zachos and Kump*, 2005] (Figure 3b), increased Southern Ocean ice-rafted debris (IRD) accumulation [e.g., *Bornhold*, 1983; *Breza and Wise Jr*., 1992], a eustatic sea level drop [*Houben et al*., 2012], and increasing proportions of illite and chlorite in Southern Ocean sediments [*Ehrmann and Mackensen*, 1992; Figure 3d]. Together, these proxies indicate the full glaciation of Antarctica from around the Eocene/Oligocene boundary (~34 Ma) onward.

In general, for a constant degassing rate, changes in global CO_2 consumption rates by silicate weathering are unlikely to be resolvable. This derives from the constraint that over long timescales, the rate of carbon removal by silicate weathering must equal the rate of carbon addition by volcanism [*Berner and Caldeira*, 1997; *Kump and Arthur*, 1997; *Caves et al*., 2016]. Unless an additional source of carbon exists (for example, metamorphic decarbonation or net organic carbon oxidation), then silicate weathering rates must have remained reasonably constant. The marine $^{87}Sr/^{86}Sr$ is thus better seen as an Sr provenance proxy; some Himalayan rocks are well known to have highly radiogenic Sr isotope ratios. This viewpoint would suggest that there has been little change in net silicate weathering rates, but rather in the efficiency with which weathering can occur at a given climate state (i.e., a given pCO_2) [*Caves et al*., 2016].

Yet over the same interval, increases in the river DSi delivery flux have been inferred from locally enhanced BSi accumulation rates in the Southern Ocean and the equatorial basins [e.g., *Baldauf and Barron*, 1990; *Ehrmann*, 1991; *Diester-Haass*, 1995]. A recent compilation of marine sediment smear slide data [*Renaudie*, 2016] also found ambivalent evidence for increased opal abundance in the late Eocene and early Oligocene at a global scale. If correct, this can be reconciled with a roughly constant silicate weathering flux if one considers that the river Si flux is not directly linked to the CO_2 consumption rate. Instead, DSi fluxes have scope to vary depending on net reaction stoichiometry; i.e., how much of the initially mobilized DSi is retained in solution. This is important for setting the δ^{30}Si of river DSi, since Si isotope fractionation occurs through the formation of secondary clay minerals [*Oelze et al*., 2015; *Ziegler et al*., 2005a, 2005b; *Frings et al*., 2016]. This means that changing the net stoichiometry of weathering reactions should alter river δ^{30}Si: for a constant initial weathering rate, the greater the fraction of Si incorporated into clays, the greater the residual DSi δ^{30}Si and the lower the net DSi flux [*Bouchez et al*., 2013]. A key parameter is therefore weathering *congruency*, i.e., the fraction of Si mobilized during primary mineral dissolution that is retained in clays.

There are several mechanisms that may alter weathering congruency. Of particular relevance here are (i) orogeny and (ii) glaciation. Small mountain streams tend to have lower δ^{30}Si [e.g., *Georg et al*., 2006b, 2007], and weathering in these regions in general tends to be characterized by greater congruency, i.e., less clay formation owing to the kinetic and thermodynamic limits imposed by short water-mineral residence and interaction times. This might suggest that the Himalayan orogeny decreased global δ^{30}Si, but this simplistic view does not account for the Himalayan foreland basin or the floodplains of central China, which appear to act as clay formation hot spots [*Ding et al*., 2011; *Frings et al*., 2015; *von Strandmann et al*., 2017], negating any

orogenic effect. Data from glaciated Icelandic catchments [*Opfergelt et al*., 2013; *Georg et al*., 2007] and from subglacial discharge of the Greenland Ice Sheet [*Hawkings et al*., 2015] demonstrate that subglacial weathering tends to be more congruent and thus produce DSi isotopically closer to the parent material (i.e., with lower δ^{30}Si values). A slight decrease in the mean DSi δ^{30}Si delivered to the ocean probably followed Antarctic glaciation as the continent switched toward a regime dominated by physical weathering (as evidenced by the Southern Ocean clay mineralogy records) [*Ehrmann and Mackensen*, 1992, Figure 3d]. However, the impact is likely to be small simply because the mass of DSi being exported from a cold-based Antarctic ice sheet was small.

Overall, it is hard to explain the Leg 199 δ^{30}Si data solely in terms of weathering changes. This does not completely preclude a minor role for weathering nor does it challenge the evidence for a change in Antarctic weathering regime. Rather, these changes might simply be minor at a global scale, or counterbalanced by other processes. Below, we argue that a reorganization of ocean circulation is the main driver of the δ^{30}Si records.

4.6. Changes in Ocean Circulation and DSi Distribution

Reconstruction of ocean circulation in the geologic past is chiefly achieved via two approaches. The first is based on the Nd isotopic composition of seawater, as recorded in different sediment phases, expressed as $\varepsilon_{Nd}(t)$ (the sample $^{143}Nd/^{144}Nd$ ratio normalized to the bulk earth and corrected for age) [*DePaolo and Wasserburg*, 1976]. In brief, the rationale behind the Nd isotope proxy is that the $\varepsilon_{Nd}(t)$ of different ocean water masses depends on the continental rocks of the catchment area that drain into each ocean basin [e.g., *Goldstein et al*., 1984]. This leads to a measurable difference in $\varepsilon_{Nd}(t)$ values between newly formed water masses. Nd has a relatively short residence time, so ε_{Nd} does not homogenize on a global scale, and intermediate and deep waters are imprinted with the Nd isotopic composition of the site of their formation. The value of ε_{Nd} at a specific location is the result of conservative water mass mixing. Hence, the Nd radiogenic isotope system can be used to infer temporal changes in water mass mixing and circulation over geological time scales [*Frank*, 2002, and references therein].

A second method exploits the stable isotopes of carbon (expressed as δ^{13}C) in benthic foraminifera to assess the relative amount of regenerated nutrients present in deep waters flowing over a given site, as the remineralization of carbon from organic matter should lower the δ^{13}C of dissolved inorganic carbon [*Sexton et al*., 2006]. Benthic foraminifera, forming their calcium carbonate shell using carbonate ions from the ambient water, record the isotopic composition of deep waters. Ocean circulation plays a major role in the distribution of δ^{13}C at depth. The longer deep waters travel away from their site of formation, the more potential remineralization of isotopically light carbon (i.e., low δ^{13}C) can influence δ^{13}C values of deep waters. Hence, gradients in benthic foraminifera δ^{13}C can be used to estimate the relative age of deep waters between different ocean basins. This rationale is essentially the same as we put forward for the use of sponge δ^{30}Si as a paleocirculation tracer.

Cenozoic ε_{Nd} records coupled with ocean circulation models [*Lunt et al*., 2012; *Marshall et al*., 1997] suggest that there was a reconfiguration of the Pacific Ocean circulation starting in the late Eocene (37 Ma onward) [*Thomas et al*., 2014]. A substantial offset between the Nd isotope composition of North Atlantic and North Pacific deep waters [*Thomas et al*., 2003, 2008] and the lack of an east-west gradient in ε_{Nd} in the tropical Pacific Ocean [*Thomas et al*., 2008] both suggest that the early Paleogene Pacific Ocean was a relatively isolated basin, with little exchange with either the Atlantic or the Tethys. Prior to ~40–42 Ma, Pacific deep waters were formed both in the North Pacific and in the Pacific sector of the Southern Ocean (i.e., the Tasman gateway did not allow deep flow until the early Oligocene) [*Stickley et al*., 2004]. After 36 Ma, ε_{Nd} values from ODP Leg 199 trend toward less radiogenic values (i.e., decreasing ε_{Nd}; Figure 5c) interpreted as a greater influence of unradiogenic Southern Ocean deep waters on the deep equatorial Pacific [*Thomas et al*., 2008]. This has been attributed to the strengthening of Southern Ocean deepwater formation in the Pacific sector due to the progressive deepening of the Tasman gateway as Australia moved farther from Antarctica [*Thomas et al*., 2008]. This interpretation is corroborated by the interbasin gradient in δ^{13}C. Over the entire Paleogene, there is no significant offset between δ^{13}C recorded in benthic foraminifera from different ocean basins (Figure 5d), and the δ^{13}C gradient increases during the Mid-Miocene (~15 Ma) [*Cramer et al*., 2009]. This observation supports the interpretation of a relatively close source of deep waters to the equatorial Pacific either from the North Pacific or from the Pacific sector of the Southern Ocean, as deep waters do not have sufficient time to acquire resolvable changes in δ^{13}C through remineralization of organic matter.

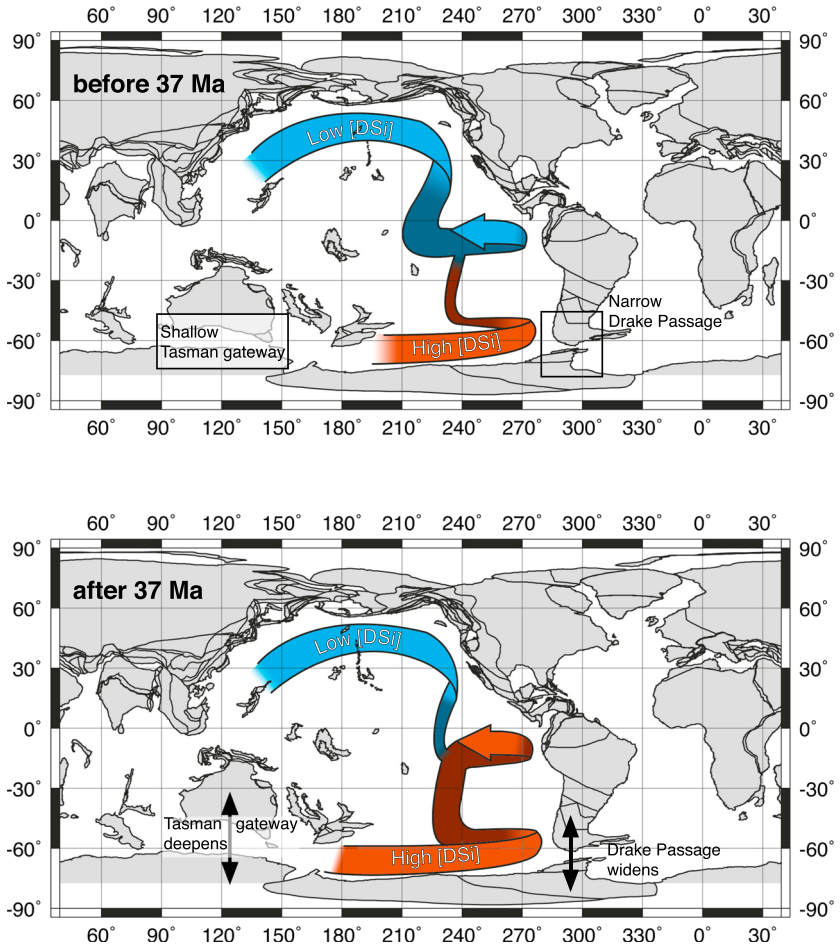

Figure 6. Schematic of inferred ocean circulation in the Pacific (top) before and (bottom) after the Eocene/Oligocene transition. Prior to 37 Ma (Figure 6, top) the Drake Passage and Tasman gateway are narrow and do not allow for a strong ACC. Deepwater transported toward the equatorial Pacific primarily originates from North Pacific deep waters (blue) with low DSi concentrations. After 37 Ma, the opening of the Drake Passage and the Tasman gateway strengthen the ACC and allow for transport of higher DSi waters originating from the Southern Ocean (red). Paleolocations of Leg 199 sites are approximately at the tip of the upwelling arrow. Plate reconstruction from *odsn.de*.

Similarly, Leg 199 sponge δ^{30}Si values decrease around 37 Ma (section 3), which to a first order reflects an increase in deepwater DSi concentrations (Figure 4) in agreement with *Egan et al.* [2013]. In isolation, this could be interpreted as either an increase in the DSi concentration of the source region or a shift in source region. As detailed above, Nd isotope records suggest a shift in the deepwater source of the equatorial Pacific coincident with the decrease of sponge δ^{30}Si values. Because the travel distance to the Leg 199 sites from both downwelling regions is similar, differential accumulation of DSi from sinking siliceous plankton is unlikely to be a large part of the explanation. Instead, the most parsimonious explanation is thus that the regions of deepwater formation in the Paleogene North and South Pacific had distinct Si biogeochemistry, i.e., with low and high [DSi], respectively. Sponge δ^{30}Si thus complements Nd isotopes and δ^{13}C gradients, two well-established paleocirculation proxies, since sponge δ^{30}Si can distinguish between water masses with different nutrient contents. While its applicability is lessened when the water masses have similar DSi concentrations (see section 4.3), the main advantage is that it contains information about the biogeochemistry of the source regions.

Considering that the equatorial Pacific was a locus of upwelling during the Paleogene [*Huber*, 2002] (Figure 1b), a noticeable change in deepwater DSi concentration should also influence the surface ocean. As a general observation, modern ocean DSi concentrations are negatively correlated to DSi δ^{30}Si. In other

words, low DSi is associated with high δ^{30}Si and vice versa, due to the fractionation associated with removal of Si from solution into biogenic silica [e.g., *De La Rocha et al*., 2000; *Varela et al*., 2004; *Cardinal et al*., 2005; *Reynolds et al*., 2006; *de Souza et al*., 2014] or alternatively due to the addition of low δ^{30}Si from dissolving diatom frustules. Radiolarian δ^{30}Si values decrease by about 0.5‰ around 34 Ma (see section 3 and Figure 3). This could be interpreted as a change in the characteristics of the upwelling waters, toward lower DSi δ^{30}Si (and potentially higher DSi concentrations), corroborating the above conclusions.

4.7. Sponge δ^{30}Si as a Paleocirculation Proxy

We suggest that the Si isotopic composition of biosiliceous remains can complement more established proxies (e.g., εNd or δ^{13}C gradients; see above) for ocean circulation. Spicule δ^{30}Si can differentiate water masses if they have distinct [DSi] but can also provide information about the nutrient content of these water masses. While further investigation of sediment from the North Pacific and the Pacific sector of the Southern Ocean would allow for the large-scale characterization of these waters, we can already make inferences about their relative DSi contents. In combination with previous work, our data indicate that prior to ~40 Ma, equatorial Pacific deep waters were mostly influenced by North Pacific deep waters forming from DSi deplete surface waters. Around 37 Ma, the source of deep water shifted from North Pacific formation to formation in the Southern Ocean where surface waters had significantly higher DSi concentrations (Figure 6). With the current data it is difficult to pinpoint why these two water masses had apparently different DSi concentrations, though analogy can be made with the modern ocean. Depletion of surface waters is easily achieved via biological uptake of DSi, providing an explanation for the low DSi northern Pacific. Conversely, high DSi waters require diatom growth limitation by at least one of the essential parameters (e.g., micronutrient or macronutrient availability and light penetration). Today, the Southern Ocean south of the Polar Front is DSi replete due to micronutrient limitation (mostly Fe) that hinders complete diatom DSi depletion [e.g., *de Baar et al*., 1990; *Franck et al*., 2000]. Demonstrating plankton Fe limitation in the Mid-Cenozoic Southern Ocean is beyond the scope of this manuscript, but if correct suggests that this is a remarkably persistent feature of ocean biogeochemistry. Further work should try to characterize these waters during the early and Mid-Cenozoic to shed light on these issues.

5. Conclusions

This study emphasizes the potential of sponge and radiolarian δ^{30}Si to reconstruct aspects of changes in ocean circulation as well as facets of the silicon cycle. We analyzed the Si isotopic composition of siliceous sponge spicules—indicative of DSi concentrations close to the ocean floor—and radiolarian tests—related to the Si isotopic composition of the upper water column—from sediment cores collected in the equatorial Pacific (ODP Leg 199) covering the Eocene and Oligocene (~48 to 23 Ma). Both sponge and radiolarian δ^{30}Si values start decreasing around 37 Ma and stabilize from 34 Ma onward. Changing the global weathering regime is unlikely to explain much of these observations. Instead, they can be interpreted as a change in the DSi concentrations in the equatorial Pacific. Specifically, the data require that the waters bathing the deep equatorial Pacific switched from Si deplete to Si replete at the end of the Eocene (~37 Ma). Previous work using ε_{Nd} has suggested that this is a period of increasing dominance of Southern Ocean deepwater formation at the expense of the North Pacific, and so the δ^{30}Si data thus corroborate this interpretation. We posit that the newly formed North Pacific deep waters had low DSi concentrations whereas the deep waters formed in the Southern Ocean had significantly higher DSi. If both conclusions are correct, this provides new information about the biogeochemistry of the Paleogene North and South Pacific. Similar work is needed to more directly characterize the water masses in the North Pacific and Southern Ocean during the Eocene and Oligocene and shed more light on the evolution of ocean circulation and nutrient distribution in the Pacific.

Acknowledgments
This work was funded by the Knut and Alice Wallenberg Foundation. Additional funding for analysis was provided by the Royal Physiographic Society of Lund. K.R.H. was funded by the Royal Society. We thank Emmanuel Ponzevera at Ifremer Brest for his support during analyses. The authors thank Donald Penman, Jill Sutton, and an anonymous reviewer for their constructive comments on an earlier version of this manuscript. Sponge and radiolarian Si isotope data can be found in the supporting information.

References

Abelmann, A., R. Gersonde, G. Knorr, X. Zhang, B. Chapligin, E. Maier, O. Esper, H. Friedrichsen, G. Lohmann, and H. Meyer (2015), The seasonal sea-ice zone in the glacial Southern Ocean as a carbon sink, *Nat. Commun.*, *6*, 8136, doi:10.1038/ncomms9136.

Amante, C., and B. W. Eakins (2009), ETOPO1 1 arc-minute global relief model: Procedures, data sources and analysis, NOAA Technical Memorandum NESDIS NGDC-24. Natl. Geophys. Data Center, NOAA, doi:10.7289/V5C8276M.

Baldauf, J. G., and J. A. Barron (1990), Evolution of biosiliceous sedimentation patterns—Eocene through quaternary: Paleoceanographic response to polar cooling, in *Geological History of the Polar Oceans: Arctic Versus Antarctic*, pp. 575–607, Springer, Netherlands.

Berner, R. A., and K. Caldeira (1997), The need for mass balance and feedback in the geochemical carbon cycle, *Geology*, *25*(10), 955–956.
Beucher, C. P., M. A. Brzezinski, and J. L. Jones (2008), Sources and biological fractionation of Silicon isotopes in the Eastern Equatorial Pacific, *Geochim. Cosmochim. Acta*, *72*(13), 3063–3073.
Beucher, C. P., M. A. Brzezinski, and J. L. Jones (2011), Mechanisms controlling silicon isotope distribution in the eastern equatorial Pacific, *Geochim. Cosmochim. Acta*, *75*(15), 4286–4294.
Bornhold, B. D. (1983), Ice-rafted debris in sediments from Leg-71, Southwest Atlantic-Ocean, *Initial Rep. Deep Sea Drill. Proj.*, *71*, 307–316.
Bouchez, J., F. Von Blanckenburg, and J. A. Schuessler (2013), Modeling novel stable isotope ratios in the weathering zone, *Am. J. Sci.*, *313*(4), 267–308.
Breza, J. R., and S. W. Wise Jr. (1992), Lower Oligocene ice-rafted debris on the Kerguelen Plateau: Evidence for East Antarctic continental glaciationin *Proc. ODP, Sci. Results*, vol. 120, edited by S. W. Wise Jr. et al., pp. 161–178, Ocean Drilling Program, College Station, Tex., doi:10.2973/odp.proc.sr.120.134.1992.
Cardinal, D., L. Y. Alleman, J. de Jong, K. Ziegler, and L. André (2003), Isotopic composition of silicon measured by multicollector plasma source mass spectrometry in dry plasma mode, *J. Anal. At. Spectrom.*, *18*(3), 213–218.
Cardinal, D., L. Y. Alleman, F. Dehairs, N. Savoye, T. W. Trull, and L. André (2005), Relevance of silicon isotopes to Si-nutrient utilization and Si-source assessment in Antarctic waters, *Global Biogeochem. Cycles*, *19*, GB2007, doi:10.1029/2004GB002364.
Carstensen, J., and A. Weydmann (2012), Tipping points in the Arctic: Eyeballing or statistical significance?, *Ambio*, *41*(1), 34–43.
Caves, J. K., A. B. Jost, K. V. Lau, and K. Maher (2016), Cenozoic carbon cycle imbalances and a variable weathering feedback, *Earth Planet. Sci. Lett.*, *450*, 152–163.
Coffineau, N., C. L. De La Rocha, and P. Pondaven (2014), Exploring interacting influences on the silicon isotopic composition of the surface ocean: A case study from the Kerguelen Plateau, *Biogeosciences*, *11*(5), 1371–1391.
Cramer, B., J. Toggweiler, J. Wright, M. Katz, and K. Miller (2009), Ocean overturning since the Late Cretaceous: Inferences from a new benthic foraminiferal isotope compilation, *Paleoceanography*, *24*, PA4216, doi:10.1029/2008PA001683.
de Baar, H. J., A. G. Buma, R. F. Nolting, G. C. Cadée, G. Jacques, and P. J. Tréguer (1990), On iron limitation of the Southern Ocean: Experimental observations in the Weddell and Scotia Seas, *Mar. Ecol. Prog. Ser.*, *65*, 105–122.
DeConto, R. M., and D. Pollard (2003), Rapid Cenozoic glaciation of Antarctica induced by declining atmospheric CO2, *Nature*, *421*(6920), 245–249.
De La Rocha, C. L. (2003), Silicon isotope fractionation by marine sponges and the reconstruction of the silicon isotope composition of ancient deep water, *Geology*, *31*(5), 423.
De La Rocha, C. L., M. A. Brzezinski, and M. J. DeNiro (1997), Fractionation of silicon isotopes by marine diatoms during biogenic silica formation, *Geochim. Cosmochim. Acta*, *61*(23), 5051–5056.
De La Rocha, C. L., M. A. Brzezinski, M. DeNiro, and A. Shemesh (1998), Silicon-isotope composition of diatoms as an indicator of past oceanic change, *Nature*, *395*(6703), 680–683.
De La Rocha, C. L., M. A. Brzezinski, and M. J. DeNiro (2000), A first look at the distribution of the stable isotopes of silicon in natural waters, *Geochim. Cosmochim. Acta*, *64*(14), 2467–2477.
de Souza, G., B. Reynolds, G. Johnson, J. Bullister, and B. Bourdon (2012), Silicon stable isotope distribution traces Southern Ocean export of Si to the eastern South Pacific thermocline, *Biogeosciences*, *9*(11), 4199–4213.
de Souza, G. F., R. D. Slater, J. P. Dunne, and J. L. Sarmiento (2014), Deconvolving the controls on the deep ocean's silicon stable isotope distribution, *Earth Planet. Sci. Lett.*, *398*, 66–76.
Demarest, M. S., M. A. Brzezinski, and C. P. Beucher (2009), Fractionation of silicon isotopes during biogenic silica dissolution, *Geochim. Cosmochim. Acta*, *73*(19), 5572–5583.
DePaolo, D., and G. Wasserburg (1976), Nd isotopic variations and petrogenetic models, *Geophys. Res. Lett.*, *3*, 249–252, doi:10.1029/GL003i005p00249.
Diester-Haass, L. (1995), Middle Eocene to early Oligocene paleoceanography of the Antarctic Ocean (Maud Rise, ODP Leg 113, Site 689): Change from a low to a high productivity ocean, *Palaeogeogr. Palaeoclimatol. Palaeoecol.*, *113*(2–4), 311–334.
Ding, T. P., J. F. Gao, S. H. Tian, H. B. Wang, and M. Li (2011), Silicon isotopic composition of dissolved silicon and suspended particulate matter in the Yellow River, China, with implications for the global silicon cycle, *Geochim. Cosmochim. Acta*, *75*(21), 6672–6689.
Egan, K. E., R. E. M. Rickaby, M. J. Leng, K. R. Hendry, M. Hermoso, H. J. Sloane, H. Bostock, and A. N. Halliday (2012), Diatom silicon isotopes as a proxy for silicic acid utilisation: A Southern Ocean core top calibration, *Geochim. Cosmochim. Acta*, *96*, 174–192.
Egan, K. E., R. E. M. Rickaby, K. R. Hendry, and A. N. Halliday (2013), Opening the gateways for diatoms primes earth for Antarctic glaciation, *Earth Planet. Sci. Lett.*, *375*, 34–43.
Ehrmann, W. U. (1991), Implications of sediment composition on the southern Kerguelen Plateau for paleoclimate and depositional environment, in *Proc. ODP, Sci. Results*, vol. 119, edited by J. Barron et al., pp. 185–210, Ocean Drilling Program, College Station, Tex., doi:10.2973/odp.proc.sr.119.121.1991.
Ehrmann, W. U., and A. Mackensen (1992), Sedimentological evidence for the formation of an East Antarctic ice sheet in Eocene/Oligocene time, *Palaeogeogr. Palaeoclimatol. Palaeoecol.*, *93*(1–2), 85–112.
Fontorbe, G., P. J. Frings, C. L. De La Rocha, K. R. Hendry, and D. J. Conley (2016), A silicon depleted North Atlantic since the Palaeogene: Evidence from sponge and radiolarian silicon isotopes, *Earth Planet. Sci. Lett.*, *453*, 67–77.
Franck, V. M., M. A. Brzezinski, K. H. Coale, and D. M. Nelson (2000), Iron and silicic acid concentrations regulate Si uptake north and south of the Polar Frontal Zone in the Pacific Sector of the Southern Ocean, *Deep Sea Res., Part II*, *47*(15–16), 3315–3338.
Frank, M. (2002), Radiogenic isotopes: Tracers of past ocean circulation and erosional input, *Rev. Geophys.*, *40*(1), 1001, doi: 10.1029/2000RG000094.
Fripiat, F., A.-J. Cavagna, N. Savoye, F. Dehairs, L. André, and D. Cardinal (2011), Isotopic constraints on the Si-biogeochemical cycle of the Antarctic Zone in the Kerguelen area (KEOPS), *Mar. Chem.*, *123*(1–4), 11–22.
Frings, P. J., W. Clymans, G. Fontorbe, W. Gray, G. J. Chakrapani, D. J. Conley, and C. De La Rocha (2015), Silicate weathering in the Ganges alluvial plain, *Earth Planet. Sci. Lett.*, *427*, 136–148.
Frings, P. J., W. Clymans, G. Fontorbe, L. Christina, and D. J. Conley (2016), The continental Si cycle and its impact on the ocean Si isotope budget, *Chem. Geol.*, *425*, 12–36.
Funakawa, S., H. Nishi, T. C. Moore, and C. A. Nigrini (2006), Data report: Late Eocene-early Oligocene radiolarians, ODP Leg 199 Holes 1218A, 1219A, and 1220A, central Pacific, in *Proceedings of the ODP, Sci. Results*, vol. 199, edited by P. A. Wilson, M. Lyle, and J. V. Firth, pp. 1–20, Ocean Drilling Program, College Station, Tex.

Garcia, H. E., R. A. Locarnini, T. P. Boyer, J. I. Antonov, O. K. Baranova, M. M. Zweng, J. R. Reagan, and D. R. Johnson (2014), *World Ocean Atlas 2013, Volume 4: Dissolved Inorganic Nutrients (phosphate, nitrate, silicate)*, edited by S. Levitus and A. Mishonov, NOAA Atlas NESDIS 76, 25 pp.
Garzione, C. N. (2008), Surface uplift of Tibet and Cenozoic global cooling, *Geology*, *36*(12), 1003–1004.
Georg, R. B., B. C. Reynolds, M. Frank, and A. N. Halliday (2006a), New sample preparation techniques for the determination of Si isotopic compositions using MC-ICPMS, *Chem. Geol.*, *235*(1–2), 95–104.
Georg, R. B., B. C. Reynolds, M. Frank, and A. N. Halliday (2006b), Mechanisms controlling the silicon isotopic compositions of river waters, *Earth Planet. Sci. Lett.*, *249*(3–4), 290–306.
Georg, R. B., B. C. Reynolds, A. J. West, K. W. Burton, and A. N. Halliday (2007), Silicon isotope variations accompanying basalt weathering in Iceland, *Earth Planet. Sci. Lett.*, *261*(3–4), 476–490.
Goldstein, S., R. O'nions, and P. Hamilton (1984), A Sm-Nd isotopic study of atmospheric dusts and particulates from major river systems, *Earth Planet. Sci. Lett.*, *70*(2), 221–236.
Grasse, P., C. Ehlert, and M. Frank (2013), The influence of water mass mixing on the dissolved Si isotope composition in the eastern equatorial Pacific, *Earth Planet. Sci. Lett.*, *380*, 60–71.
Hawkings, J. R., J. L. Wadham, M. Tranter, E. Lawson, A. Sole, T. Cowton, and J. Telling (2015), The effect of warming climate on nutrient and solute export from the Greenland ice Sheet, *Geochem. Perspect. Lett*, *1*, 94–104.
Hendry, K. R., and L. F. Robinson (2012), The relationship between silicon isotope fractionation in sponges and silicic acid concentration: Modern and core-top studies of biogenic opal, *Geochim. Cosmochim. Acta*, *81*, 1–12.
Hendry, K. R., L. F. Robinson, J. F. McManus, and J. D. Hays (2014), Silicon isotopes indicate enhanced carbon export efficiency in the North Atlantic during deglaciation, *Nat. Commun.*, *5*, 3107, doi:10.1038/ncomms4107.
Hendry, K., G. E. Swann, M. J. Leng, H. J. Sloane, C. Goodwin, J. Berman, and M. Maldonado (2015), Technical Note: Silica stable isotopes and silicification in a carnivorous sponge *Asbestopluma* sp, *Biogeosciences*, *12*(11), 3489–3498.
Houben, A. J., C. A. van Mourik, A. Montanari, R. Coccioni, and H. Brinkhuis (2012), The Eocene–Oligocene transition: Changes in sea level, temperature or both?, *Palaeogeogr. Palaeoclimatol. Palaeoecol.*, *335*, 75–83.
Huber, M. (2002), Straw man 1: A preliminary view of the tropical Pacific from a global coupled climate model simulation of the early Paleogene, in *Proc. ODP, Init. Repts.*, vol. 199, edited by M. Lyle et al., pp. 1–30, Ocean Drilling Program, College Station, Tex.
Kamikuri, S.-I., H. Nishi, T. C. Moore, C. A. Nigrini, and I. Motoyama (2005), 4. Data report: Late Oligocene and Early Miocene radiolarians, sites 1218 and 1219, Central Pacific, in *Proceedings of the ODP, Sci. Results*, vol. 199, edited by P. A. Wilson, M. Lyle, and J. V. Firth, pp. 1–13, Ocean Drilling Program, College Station, Tex.
Krabberød, A. K., J. Bråte, J. K. Dolven, R. F. Ose, D. Klaveness, T. Kristensen, K. R. Bjørklund, and K. Shalchian-Tabrizi (2011), Radiolaria divided into Polycystina and Spasmaria in combined 18S and 28S rDNA phylogeny, *PLoS One*, *6*(8), e23526.
Kump, L. R., and M. A. Arthur (1997), Global chemical erosion during the Cenozoic: Weatherability balances the budgets, *Tectonic Uplift Clim. Change*, 399–426.
Lazarus, D. B., B. Kotrc, G. Wulf, and D. N. Schmidt (2009), Radiolarians decreased silicification as an evolutionary response to reduced Cenozoic ocean silica availability, *Proc. Natl. Acad. Sci. U.S.A.*, *106*(23), 9333–9338.
Lear, C. H., T. R. Bailey, P. N. Pearson, H. K. Coxall, and Y. Rosenthal (2008), Cooling and ice growth across the Eocene-Oligocene transition, *Geology*, *36*(3), 251–254.
Lunt, D. J., T. Dunkley Jones, M. Heinemann, M. Huber, A. LeGrande, A. Winguth, C. Loptson, J. Marotzke, C. Roberts, and J. Tindall (2012), A model–data comparison for a multi-model ensemble of early Eocene atmosphere–ocean simulations: EoMIP, *Clim. Past*, *8*, 1717–1736.
Lyle, M., et al. (2002), *Proceedings of the ODP, Init. Rep*, vol. 199, Ocean Drilling Program, College Station, Tex.
Maliva, R. G., A. H. Knoll, and R. Siever (1989), Secular change in chert distribution: A reflection of evolving biological participation in the silica cycle, *Palaios*, *4*, 519–532.
Marin-Carbonne, J., F. Robert, and M. Chaussidon (2014), The silicon and oxygen isotope compositions of Precambrian cherts: A record of oceanic paleo-temperatures?, *Precambrian Res.*, *247*, 223–234.
Marshall, J., A. Adcroft, C. Hill, L. Perelman, and C. Heisey (1997), A finite-volume, incompressible Navier stokes model for studies of the ocean on parallel computers, *J. Geophys. Res.*, *102*, 5753–5766, doi:10.1029/96JC02775.
Morley, D. W., M. J. Leng, A. W. Mackay, H. J. Sloane, P. Rioual, and R. W. Battarbee (2004), Cleaning of lake sediment samples for diatom oxygen isotope analysis, *J. Paleolimnol.*, *31*(3), 391–401.
Oelze, M., F. von Blanckenburg, J. Bouchez, D. Hoellen, and M. Dietzel (2015), The effect of al on Si isotope fractionation investigated by silica precipitation experiments, *Chem. Geol.*, *397*, 94–105.
Opfergelt, S., K. W. Burton, P. P. von Strandmann, S. R. Gislason, and A. N. Halliday (2013), Riverine silicon isotope variations in glaciated basaltic terrains: Implications for the Si delivery to the ocean over glacial–interglacial intervals, *Earth Planet. Sci. Lett.*, *369*, 211–219.
Palmer, M. R., and H. Elderfield (1985), Sr isotope composition of sea water over the past 75 Myr, *Nature*, *314*(6011), 526–528.
Panizzo, V. N., G. E. A. Swann, A. W. Mackay, E. Vologina, M. Sturm, V. Pashley, and M. S. A. Horstwood (2016), Insights into the transfer of silicon isotopes into the sediment record, *Biogeosciences*, *13*(1), 147–157.
Rabosky, D. L., and U. Sorhannus (2009), Diversity dynamics of marine planktonic diatoms across the Cenozoic, *Nature*, *457*(7226), 183–186.
Raymo, M. E., and W. F. Ruddiman (1992), Tectonic forcing of late Cenozoic climate, *Nature*, *359*(6391), 117–122.
Renaudie, J. (2016), Quantifying the Cenozoic marine diatom deposition history: Links to the C and Si cycles, *Biogeosciences*, *13*(21), 6003–6014.
Reynolds, B. C., M. Frank, and A. N. Halliday (2006), Silicon isotope fractionation during nutrient utilization in the North Pacific, *Earth Planet. Sci. Lett.*, *244*(1–2), 431–443.
Reynolds, B. C., J. Aggarwal, L. André, D. Baxter, C. Beucher, M. A. Brzezinski, E. Engström, R. B. Georg, M. Land, and M. J. Leng (2007), An inter-laboratory comparison of Si isotope reference materials, *J. Anal. At. Spectrom.*, *22*(5), 561–568.
Rowley, D. B. (2002), Rate of plate creation and destruction: 180 ma to present, *Geol. Soc. Am. Bull.*, *114*(8), 927–933.
Sexton, P. F., P. A. Wilson, and R. D. Norris (2006), Testing the Cenozoic multisite composite $\delta^{18}O$ and $\delta^{13}C$ curves: New monospecific Eocene records from a single locality, Demerara Rise (Ocean Drilling Program Leg 207), *Paleoceanography*, *21*, PA2019, doi:10.1029/2005PA001253.
Siever, R. (1991), Silica in the oceans: Biological-geochemical interplay, *Scientists on Gaia*, 287–295.
Stickley, C. E., H. Brinkhuis, S. A. Schellenberg, A. Sluijs, U. Röhl, M. Fuller, M. Grauert, M. Huber, J. Warnaar, and G. L. Williams (2004), Timing and nature of the deepening of the Tasmanian gateway, *Paleoceanography*, *19*, PA4027, doi:10.1029/2004PA001022.
Sun, X., M. Olofsson, P. S. Andersson, B. Fry, C. Legrand, C. Humborg, and C. M. Mörth (2014), Effects of growth and dissolution on the fractionation of silicon isotopes by estuarine diatoms, *Geochim. Cosmochim. Acta*, *130*, 156–166.

Sutton, J. N., D. E. Varela, M. A. Brzezinski, and C. P. Beucher (2013), Species-dependent silicon isotope fractionation by marine diatoms, *Geochim. Cosmochim. Acta*, *104*, 300–309.

Tatzel, M., F. von Blanckenburg, M. Oelze, J. A. Schuessler, and G. Bohrmann (2015), The silicon isotope record of early silica diagenesis, *Earth Planet. Sci. Lett.*, *428*, 293–303.

Thomas, D. J., T. J. Bralower, and C. E. Jones (2003), Neodymium isotopic reconstruction of late Paleocene–early Eocene thermohaline circulation, *Earth Planet. Sci. Lett.*, *209*(3–4), 309–322.

Thomas, D. J., M. Lyle, T. C. Moore, and D. K. Rea (2008), Paleogene deepwater mass composition of the tropical Pacific and implications for thermohaline circulation in a greenhouse world, *Geochem. Geophys. Geosyst.*, *9*, Q02002, doi:10.1029/2007GC001748.

Thomas, D. J., R. Korty, M. Huber, J. A. Schubert, and B. Haines (2014), Nd isotopic structure of the Pacific Ocean 70-30 ma and numerical evidence for vigorous ocean circulation and ocean heat transport in a greenhouse world, *Paleoceanography*, *29*, 454–469, doi:10.1002/2013PA002535.

Varela, D. E., C. J. Pride, and M. A. Brzezinski (2004), Biological fractionation of silicon isotopes in Southern Ocean surface waters, *Global Biogeochem. Cycles*, *18*, GB1047, doi:10.1029/2003GB002140.

von Strandmann, P. A. P., P. J. Frings, and M. J. Murphy (2017), Lithium isotope behaviour during weathering in the Ganges Alluvial Plain, *Geochim. Cosmochim. Acta*, *198*, 17–31.

Wallace, A. F., D. Wang, L. M. Hamm, A. H. Knoll, and P. M. Dove (2012), Eukaryotic skeletal formation, in *Fundamentals of Geobiology*, pp. 150–187, John Wiley, Chichester, U. K.

Wetzel, F., G. De Souza, and B. Reynolds (2014), What controls silicon isotope fractionation during dissolution of diatom opal?, *Geochim. Cosmochim. Acta*, *131*, 128–137.

Wille, M., J. Sutton, M. J. Ellwood, M. Sambridge, W. Maher, S. Eggins, and M. Kelly (2010), Silicon isotopic fractionation in marine sponges: A new model for understanding silicon isotopic variations in sponges, *Earth Planet. Sci. Lett.*, *292*(3–4), 281–289.

Zachos, J., M. Pagani, L. Sloan, E. Thomas, and K. Billups (2001), Trends, rhythms, and aberrations in global climate 65 ma to present, *Science*, *292*(5517), 686–693.

Zachos, J. C., and L. R. Kump (2005), Carbon cycle feedbacks and the initiation of Antarctic glaciation in the earliest Oligocene, *Global Planet. Change*, *47*(1), 51–66.

Zachos, J. C., B. N. Opdyke, T. M. Quinn, C. E. Jones, and A. N. Halliday (1999), Early cenozoic glaciation, antarctic weathering, and seawater 87Sr/86Sr: Is there a link?, *Chem. Geol.*, *161*(1–3), 165–180.

Ziegler, K., O. A. Chadwick, M. A. Brzezinski, and E. F. Kelly (2005a), Natural variations of δ^{30}Si ratios during progressive basalt weathering, Hawaiian Islands, *Geochim. Cosmochim. Acta*, *69*(19), 4597–4610.

Ziegler, K., O. A. Chadwick, A. F. White, and M. A. Brzezinski (2005b), δ^{30}Si systematics in a granitic saprolite, Puerto Rico, *Geology*, *33*(10), 817–820.